

Long-wavelength UV-LEDs and charge management in the detection of gravitational waves in space

Yuandong Jia^{1,2}, Yinbowen Zhang², Suwen Wang³, Guozhi Chai², Zemin Zhang², Yi Zhang⁴, Hongxin Li⁵, Shuanglin Huang⁶, Hongqing Huo^{2,*}, Zongfeng Li^{7,*} and Yun Kau Lau⁸

¹ School of Physics and Photoelectric Engineering, Key Laboratory of Gravitational Wave Precision Measurement of Zhejiang Province, Taiji Laboratory for Gravitational Wave Universe, Hangzhou Institute for Advanced Study, University of Chinese Academy of Sciences, Hangzhou, China

² School of Physical Science and Technology, Lanzhou University, Lanzhou, China

³ Hainan Tropical Ocean University, Sanya, China

⁴ School of Nuclear Science and Technology, Lanzhou University, Lanzhou, China

⁵ School of Information Science & Engineering, Lanzhou University, Lanzhou, China

⁶ Beijing Institute of Mathematical Sciences and Applications, Beijing, China

⁷ Key Laboratory of Space Utilization, Technology and Engineering Center for Space Utilization, Chinese Academy of Sciences, Beijing, China

⁸ Innovation Academy for Microsatellites, Key Lab for Satellite Digitalization Technology, Chinese Academy of Sciences, Shanghai, 201203, China.

Correspondence*:

Hongqing Huo
huohq@lzu.edu.cn

Zongfeng Li
lzfeng@csu.ac.cn

ABSTRACT

For the charge management system in gravitational wave detection missions, a continuous discharge strategy is considered by continuously illuminating a test mass (TM) with weak light in such a way to strike a balance between the charging and discharging rates and at the same time avoids the requirement for frequent activation of charge measurements. Built on experiments by one of us Wang et al. (2022) based on a simple parallel plate model for inertial sensor, in the present work a more sophisticated inertial sensor model that mimics the surface properties and work function of a cubical TM of an inertial sensor in space (like that of the LISA Pathfinder) is employed to study bipolar charge management system that utilizes UV-LEDs with peak wavelengths of 269 nm, 275 nm, 280 nm, and 295 nm that are longer than the standard 255 nm commonly employed for direct TM illumination. Experimental results indicate that the 275 nm UV-LED achieves optimal performance, maintaining the TM potential closer to zero and at the same time accommodates both rapid discharge and continuous discharge strategies. The present work provides useful input in the future study of system design and optimization for the charge management system.

Keywords: UV-LED, charge management, inertial sensors, passive charge control, discharge strategy

1 INTRODUCTION

In gravitational wave detection in space, spacecraft is exposed to the heliospheric environment and subjected to continuous bombardment by high energy particles Jafry et al. (1996); Armano et al. (2023); Araújo et al. (2005). When the energies exceed a certain threshold, particles will penetrate the spacecraft and deposit on a TM, generating spurious acceleration noise and disturbing gravitational wave detection Carbone et al. (2004); Sumner et al. (2020). Beginning from the Gravity Probe B(GP-B) mission and later on the LISA Pathfinder(LPF), photoelectric effect is employed as a non-contact way to neutralise charges where the mercury lamp is used as the ultraviolet(UV) light source Buchman et al. (1995); Sumner et al. (2009); Wass et al. (2006); Armano et al. (2017). Instead of mercury lamp, UV-LED is considered as a better alternative for a number of technical reasons in the upcoming LISA and the prospective Chinese missions, such as TaiJi and TianQin Olatunde et al. (2015); Hu and Wu (2017); Luo et al. (2016). UV-LED based charge management systems are now widely studied, and Stanford University has successfully demonstrated charge management system with UV-LEDs in space Saraf et al. (2016); Hollington et al. (2015); Yang et al. (2020); Wang et al. (2022).

During a solar cycle, charge control strategies vary with particle flux intensity. Among them, continuous discharge is used to balance the charging-discharging rates, typically suited for the ascending and descending phase of a solar cycle in which particle flux is predominantly due to galactic cosmic rays and the solar activity is low. A continuous discharge method employing dual UV light sources was proposed to illuminate both the TM and the electrode housing, effectively maintaining the TM potential near zero Pi et al. (2023); Wang et al. (2022); Armano et al. (2018). Previously, Wang and the Stanford group studied continuous charge management methods by employing UV light with a peak wavelength longer than the 255 nm commonly used, and they used a simplified parallel plate model derived from an inertial sensor Wang et al. (2022).

The aim of the present work is to conduct this study by employing a more realistic model of an inertial sensor instead of a simple parallel plate model. A cubic TM is fixed within an electrode housing via insulating pillars and the surfaces are gold coated to mimic those of the LPF in terms of the work function and surface properties of the TM as well as the electrode housing. Continuous discharge requires sustained operation during solar minimum periods. However, constrained by the experimental conditions of this study, we use 4-hour continuous discharge results to demonstrate in a preliminary way its performance, corresponding to the 0.1 mHz frequency band essential for space-based gravitational wave detection. A preliminary continuous charge management is then studied using multiple wavelengths of UV-LEDs. Experimental results indicate that, due to internal reflections of UV light within the electrical housing, the photoelectron emission is different from that of a parallel plate model. Further, our results show that 275 nm outperforms the standard 255 nm wavelength for both fast release of charged particles as well as for continuous charge management, it is capable of achieving smaller equilibrium potential with long time stability.

In the present work, we investigate the UV-LED light sources for charge management. Although these light sources have been extensively studied by a number of research groups with focus on the 255 nm wavelength. Our contribution lies in exploring longer wavelength light sources beyond conventional 255 nm, and we argue that during periods of low solar activity, the 275 nm light source seems to be a better option. This result is similar to our previous experiments based on UV micro-LED light sources(Jia et al. (2025)), where we used four UV micro-LEDs of different wavelengths. Light sources with wavelengths longer than the 255 nm commonly used achieved a equilibrium potential closer to 0 mV, with 274 nm reaching -10 mV. However, in the paper(Jia et al. (2025)), we focus more on the feasibility of applying this new light source

to charge management in the detection of gravitational wave in space. We conducted a characterization analysis of the new light source and verified its potential application in the space environment.

The present work is structured as follows. In section 2, charge management model based on a UV-LED with long wavelength is introduced and analyzed. In section 3, based on the cubic charge management system, photoelectric effect for a UV-LED with peak wavelength of 275 nm is demonstrated. Continuous charge control using UV-LEDs with different peak wavelengths will be studied in section 4, which will enable us to explore a method using light sources different from the standard 255 nm. The experimental results show that UV-LEDs with longer wavelengths achieve excellent long-term stability, maintaining equilibrium potentials within approximately 50 mV over a four-hour period, and achieving a charge noise level of $10^{-13} \text{ C}/\sqrt{\text{Hz}}$ near 0.1 mHz. Moreover, 275 nm UV-LED achieves not only smaller equilibrium potential (-12 mV) but also faster discharge rate (6 s), making it a promising candidate as a better light source for charge management system.

2 PRINCIPLE OF CHARGE MANAGEMENT

In this section, we will present a charge management model for long-wavelength UV-LED illumination, on the basis of which we try to understand our experimental results and perform data analysis.

Fig. 1 presents a schematic representation of the charge management mechanism employing long-wavelength (i.e., wavelength longer than 255 nm) UV-LED for direct illumination. The work function of Au exposed to air is approximately 4.2 eV Schulte et al. (2009); Jiang et al. (1998). As a result, incident light with a photon energy greater than 4.2 eV (corresponding to a wavelength of less than 295 nm) is sufficient to induce photoemission for charge management. In this configuration, UV light illuminates the TM and reflects between the TM and the electrode housing (EH). Photoelectrons are subsequently emitted from both gold-coated surfaces.

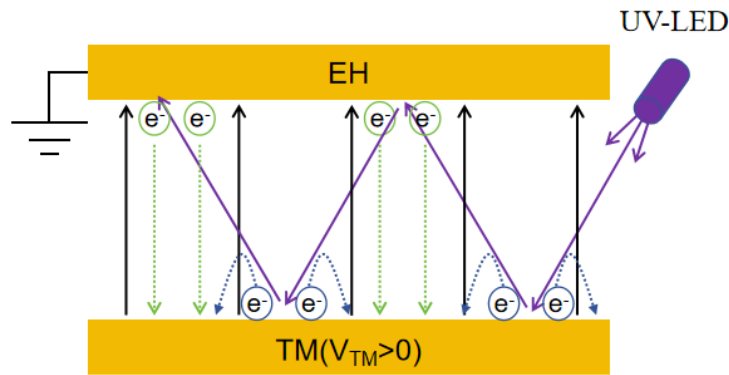


Figure 1. A schematic of photoelectron migration when the potential of the TM is positive and greater than the initial kinetic energy of the photoelectrons.

Consider the case in which the potential of the TM is positive and greater than the initial kinetic energy of the photoelectrons, where the electrode housing (including its mounted electrodes) is grounded. the presence of the local electric field causes photoelectrons to migrate to the TM, thereby reducing its potential, as shown in Fig. 1. When the potential approaches zero and becomes comparable to the initial kinetic energy of the photoelectrons, the photoelectron flow between the TM and the electrode housing reaches an equilibrium state. At this point, the TM attains a stable potential, as illustrated in Fig. 2. A similar

process occurs when the initial TM charge is negative. As the wavelength of the incident light increases, the photon energy decreases, which correspondingly reduces the kinetic energy of the generated photoelectrons. Thereby, a smaller equilibrium potential of the TM can be achieved.

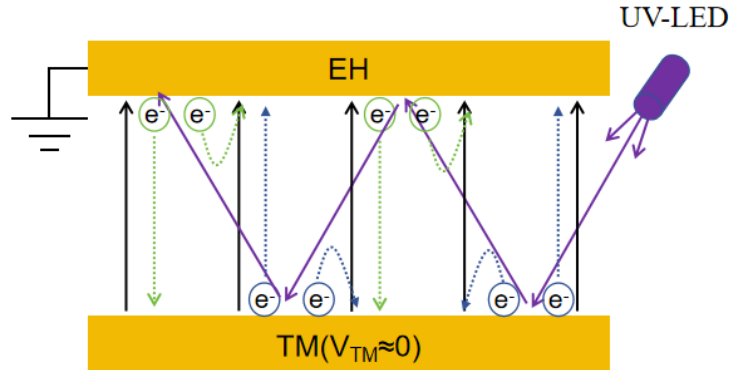


Figure 2. A schematic of photoelectron migration when the potential of the TM approaches zero and becomes comparable to the initial kinetic energy of the photoelectrons

The application of a bias voltage (V_B) to the electrode will influence the migration of photoelectrons between the TM and the electrode housing. The potential variation of the TM under UV illumination follows an exponential function, which has been verified through both theoretical modeling and experimental validation Pi et al. (2023); Li et al. (2025):

$$V_{TM}(t) = Ae^{-\frac{t}{\tau}} + V_{eq}(V_B) \quad (1)$$

where τ is the time constant that reflects the potential variation rate of the TM, and $V_{eq}(V_B)$ is the equilibrium potential to which the TM will settle under a given bias voltage after prolonged illumination.

3 GROUND EXPERIMENTS OF CHARGE MANAGEMENT.

3.1 Experimental setup

In this work, instead of the parallel plate model, we conducted experiments using a cubic TM enclosed in an electrical housing, as in the case of the LISA Pathfinder mission. This enables us to evaluate the performance of UV-LEDs in a setting that closely resembles that on orbit.

Fig. 3 illustrates the experiment setup for validating long-wavelength UV-LED based charge management systems. The vacuum chamber maintained an operational pressure on the order of 10^{-4} Pa throughout testing. The electrical housing model was designed to mimic the inertial sensor of LISA Pathfinder, featuring a measured TM-to-surroundings capacitance of 28.8 pF. Both the surface of the TM and the inner surface of the electrode housing were gold-coated to a thickness of 500 nm Saraf et al. (2014). The TM was fixed inside the electrode housing using insulated Ultem-1000 holding tubes, which provided a TM-to-EH resistance on the order of 10^{14} Ω . UV-LEDs were mounted at the upper vertices of the housing, providing direct illumination on the TM. A contact probe mounted at the centre of the upper surface of the TM was used for real-time potential measurements with an accuracy of 0.1 mV, while the bias electrode was either grounded or connected to an external voltage source to provide a bias potential. This configuration deviates

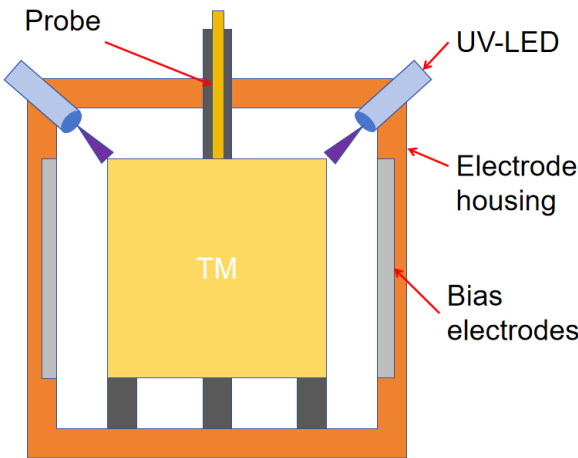


Figure 3a. Schematic.

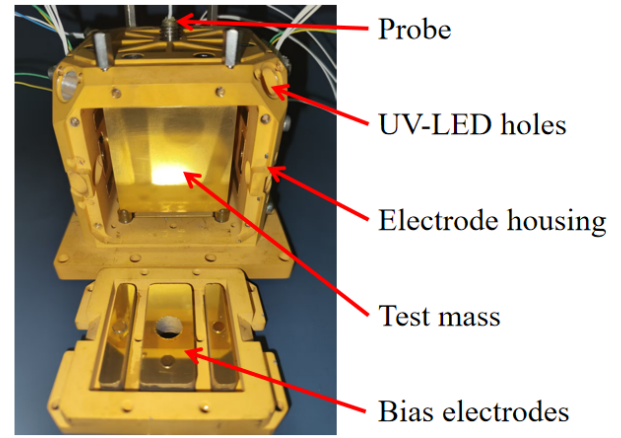


Figure 3b. Photograph.

Figure 3. Experiment setup of the charge management system. **(A)** Schematic. **(B)** Photograph.

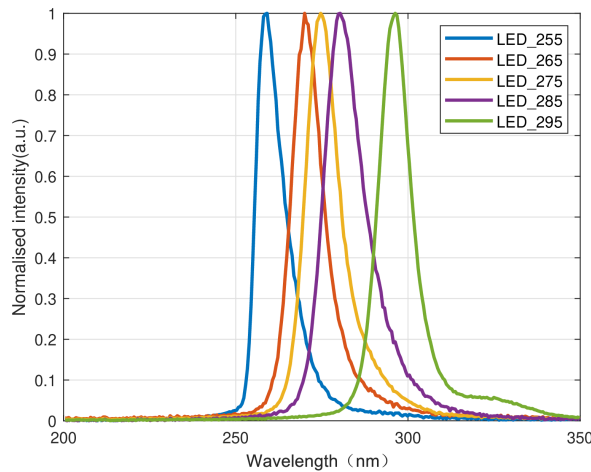


Figure 4a. Emission spectra of the UV-LEDs.

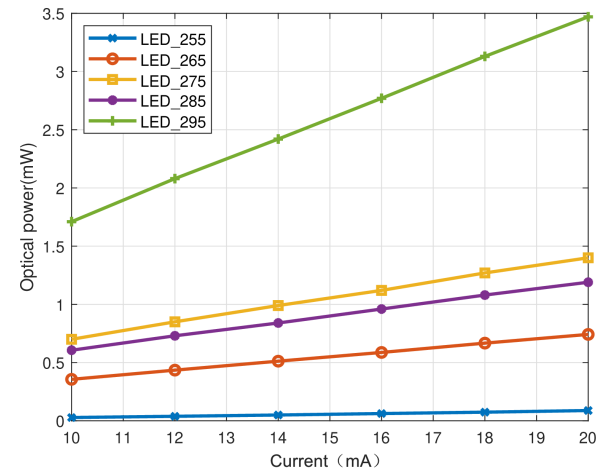


Figure 4b. P-I curve of the UV-LEDs.

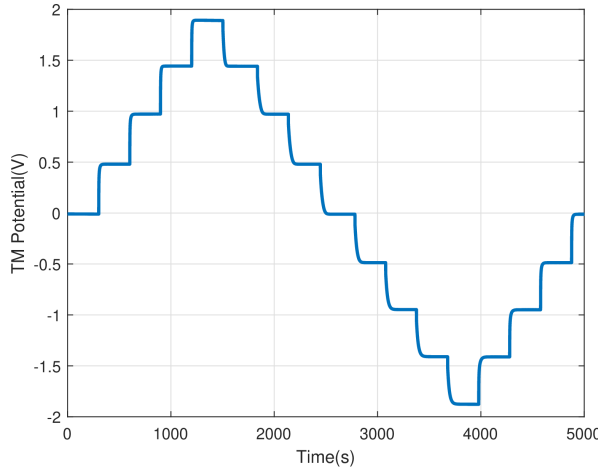
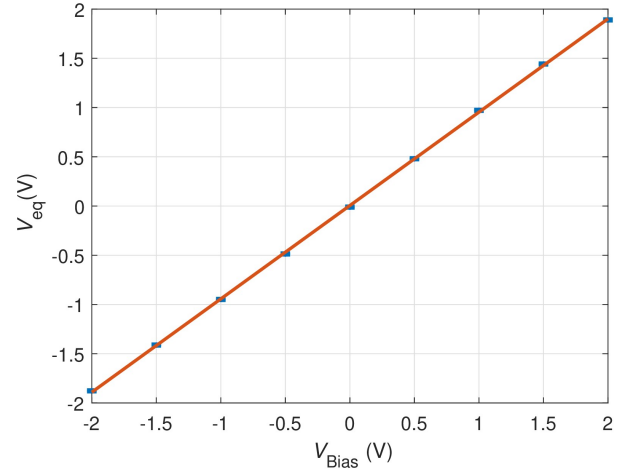
Figure 4. Characteristic performance of the five UV-LEDs in the experiment. **(A)** Emission spectra. **(B)** P-I curve.

from the previous simple two parallel plates model and allows for a comprehensive analysis of the charge management process under conditions that closely mimic those encountered in actual space missions.

Fig. 4 presents the emission spectra and optical power versus current (P-I) of the five UV-LEDs used in this study. During the P-I curve measurements, the power meter was positioned at a distance of 3 cm from the UV-LEDs. Table 1 summarizes the peak wavelengths and full width at half maximum (FWHM) values for all five UV-LEDs.

Table 1. Characteristics of the UV-LEDs used in the experiment

LED	Peak wavelength(nm)	FWHM(nm)	Manufacturer	Part number
LED_255	259.1 \pm 0.5	9 \pm 1	NewOpto	UVLED255-TO39HS
LED_265	269.4 \pm 0.5	10 \pm 1	NewOpto	UVLED265-TO39HS
LED_275	274.6 \pm 0.5	11 \pm 1	NewOpto	UVLED275-TO39HS
LED_285	280.3 \pm 0.5	13 \pm 1	NewOpto	UVLED285-TO39HS
LED_295	296.3 \pm 0.5	11 \pm 1	NewOpto	UVLED295-TO39HS

**Figure 5a.** V_{TM} as a function of time with V_B .**Figure 5b.** V_{eq} as a function of V_B .**Figure 5.** Demonstration of the variation of V_{TM} affected by V_B under the illumination of LED_275. (A) V_{TM} as a function of time with V_B varied from -2 V to 2 V in steps of 0.5 V. (B) V_{eq} as a function of V_B .

3.2 Photoelectrons emission.

To study the charge control capability of the system, two experimental runs were conducted using the LED_275. In these experiments, an increase in the potential of the TM was defined as charging, while a decrease was defined as discharging. Fig. 5 illustrates the correlation between the bias electrode potential (V_B) and the TM potential (V_{TM}), while the UV-LED drive current was maintained at 10 mA during the measurements.

A continuous test was conducted by sweeping V_B from 0 V to +2 V, then to -2 V, and finally returning to 0 V in steps of 0.5 V. Each voltage setting was maintained for 300 seconds while monitoring V_{TM} until reaching equilibrium (Fig. 5a). Based on (1), the equilibrium potentials of the TM V_{eq} corresponding to nine discrete V_B configurations are plotted in Fig. 5b, where the solid line represents the fit to the data:

$$V_{eq} (V) = (0.948 \pm 0.004) \times V_B (V) + (0.005 \pm 0.005) (V) \quad (2)$$

The R^2 of the fitting is 0.99989, the slope is 0.948 with a 95% confidence interval (CI) of [0.939, 0.957], and the intercept is 0.005 V with a 95% CI of [-0.006, 0.017] V.

The charge management system performance was also influenced by the UV-LED drive current. In this experiment, the LED_275 drive current was set to 10 mA, 15 mA and 20 mA respectively while the bias electrode was either grounded or set to $V_B = 1$ V. The corresponding TM potential variations are

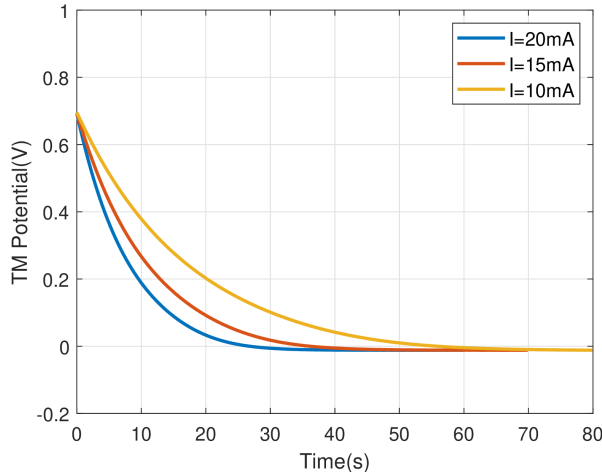


Figure 6a. The bias electrode was grounded.

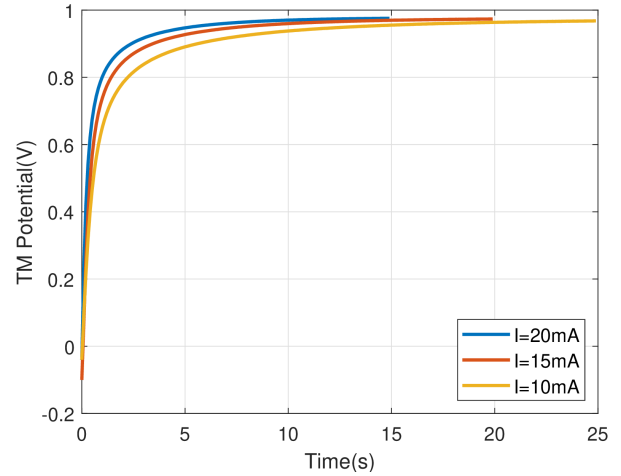


Figure 6b. V_{eq} as a function of V_B .

Figure 6. TM potential variation for LED_275 with drive currents of 10 mA, 15 mA, and 20 mA. (A) The bias electrode was grounded. (B) The potential of bias electrode was set to 1 V.

Table 2. Maxima of potential variations under different currents for the charging and discharging from Fig. 6.

I(mA)	$(dV/dt)^-$ (mV/s)	I (pA)	$(dV/dt)^+$ (mV/s)	I (pA)
10	84.5	2.43	2314	66.6
15	61.6	1.78	1793	51.6
20	39.5	1.13	1290	37.2

presented in Figure 6. The experimental results reveal an inverse relationship between the UV-LED drive current and the stabilization time of the TM potential, while the equilibrium potential is independent of it. Table 2 summarizes the maxima variation of TM potential at the start of discharge $(dV/dt)^-$ and charging $(dV/dt)^+$ with about 5% uncertainty for the three sets of drive current. It should be noted that the discharge rate differs from the charging rate by a factor of about 30. This discrepancy arises from two main aspects: first, the net photoelectron flux between the TM and the electrode housing depends on the potential polarity of the TM; second, it is influenced by the difference between the initial potential and the equilibrium potential of the TM.

4 CONTINUOUS CHARGE CONTROL.

In this experiment, long-wavelength UV-LEDs were used to evaluate the charge management performance. The performance was quantified by three metrics: the equilibrium potential of the TM, the stability of this potential, and the discharge rate.

Fig. 7 illustrates the equilibrium potential V_{eq} as a function of the bias electrode potential V_B under illumination by UV-LEDs of five different wavelengths. The zero-bias regime ($V_B = 0$ V) represents the primary focus of this study, with its detailed characteristics highlighted in the enlarged inset in the upper-left corner.

The equilibrium potential of the TM under zero-bias conditions ($V_B = 0$ V) was used to quantify the charge management performance. Table 3 summarizes these measurements (corresponding to the shaded

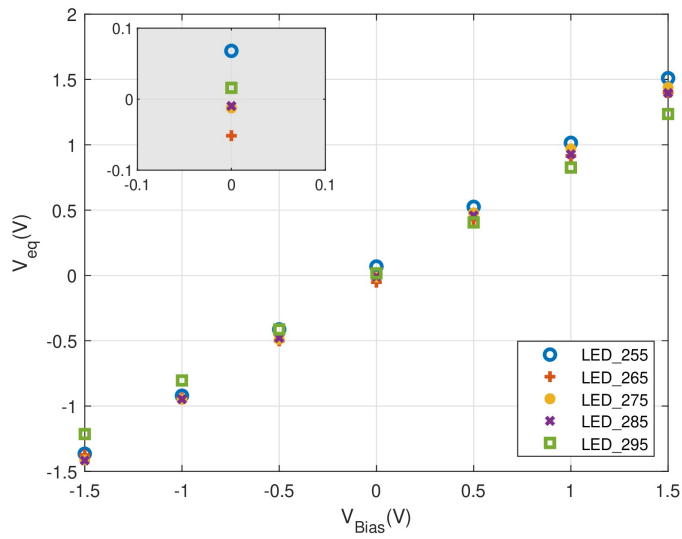


Figure 7. TM equilibrium potential as a function of the bias potential for different wavelength UV-LEDs

Table 3. TM equilibrium potential under illumination by UV-LEDs of different wavelengths.

LED	Equilibrium potential(mV)
LED_255	68.4 ± 0.6
LED_265	-51.5 ± 0.2
LED_275	-12.0 ± 0.2
LED_285	-9.9 ± 0.8
LED_295	16.1 ± 1.1

insert in figure 7), demonstrating that direct TM illumination enables continuous charge control. The results show that all five UV-LEDs maintain the TM charge within ± 100 mV, the LISA requirement (equivalent to about 2×10^7 elementary charges Antonucci et al. (2012)). It should be noted that LED_255 and LED_265 achieve comparable equilibrium potentials around 50 mV, while the longer LED_275, LED_285, and LED_295 are moving the TM significantly closer to zero potential, indicating superior performance in precision charge management. It should be noted that the polarity of the equilibrium potential varies under different UV-LEDs. This is because the equilibrium potential is governed by the net photoelectron flux between the TM and the electrode housing, which in turn is influenced by factors such as the incident light wavelength, the geometry of the electrode housing, and the physical properties of the gold-coated surfaces. Therefore, further investigation through simulation is required to fully understand the behaviour of the equilibrium potential.

To evaluate the temporal stability of the long-wavelength UV-LED-based charge management system, four-hour continuous tests were conducted using LED_265, LED_275, LED_285 and LED_295. During these tests, the drive current was set to 10 mA, and the bias electrode was grounded. Fig. 8(a) illustrates V_{TM} over time for each wavelength, and Fig. 8(b) shows the equivalent TM charge noise under the control of the LED_275.

The experimental results demonstrate stable maintenance of the TM potential within ± 100 mV of the target value over the 4-hour duration, with all four wavelengths exhibiting peak-to-peak fluctuations below 2 mV. This confirms the viability of long-wavelength UV-LEDs for passive charge management

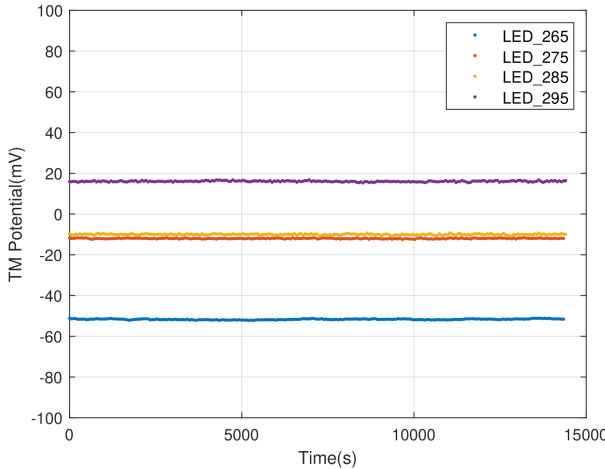


Figure 8a. TM potential drift about 4 hours.

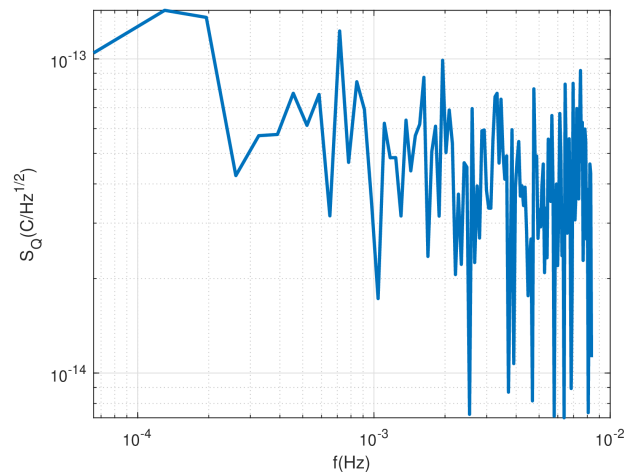


Figure 8b. V_{eq} as a function of V_B .

Figure 8. Experiment results of long-wavelength UV-LED-based charge management system. (A) TM potential drift about 4 hours. (B) TM charge noise under the control of the LED_275.

Table 4. Time constant for different wavelength UV-LEDs.

LED	Time constant(s)	Calibrated Time constant(s)
LED_265	10.16 ± 0.08	3.62 ± 0.08
LED_275	8.58 ± 0.04	6.01 ± 0.07
LED_285	49.4 ± 0.2	29.9 ± 0.4
LED_295	386 ± 3	660 ± 24

in gravitational reference sensor applications. Under the control of the LED_275, the system achieved a charge noise level of $10^{-13} \text{ C}/\sqrt{\text{Hz}}$ near 0.1 mHz , corresponding to an equivalent acceleration noise of $10^{-15} \text{ m} \cdot \text{s}^{-2}/\sqrt{\text{Hz}}$ as derived from the literature Sumner et al. (2020). Subsequently, we will conduct longer-duration continuous discharge experiments, including tests at lower frequency bands with both charge management on and charge management off, thereby validating its capability for sustained operation throughout the entire mission duration. And the 4-hour test duration is relatively brief compared to a full space mission cycle, and additional risks may exist in long-term missions such as space gravitational wave detection (e.g., device aging, performance drift, etc.). Future ground-based experiments will be conducted over extended periods to simulate the complete mission cycle.

To evaluate the charging rate of V_{TM} for long-wavelength UV-LED illumination, experiments were conducted using LED_265, LED_275, LED_285, and LED_295. The UV-LED drive current was set to 10 mA, and the bias electrode was grounded during measurements. Fig. 10 shows the V_{TM} variation. By fitting V_{TM} with time using 2, time constants for each wavelength are summarized in Table 4. As shown in Figure 4, the four UV-LEDs exhibit distinct optical powers at a drive current of 10 mA. Given the inverse proportionality between time constants and optical power, Table 4 also lists the time constants normalized relative to a reference optical power of 1 mW for each UV-LED.

As shown in Table 4, the time constant after calibration increases with wavelength. The time constants of LED_285 and LED_295 are significantly larger than those of LED_265 and LED_275. Under conditions normalized to 1 mW output power and identical TM potentials, LED_265 and LED_275 stabilize the potential near equilibrium within 6 seconds. In contrast, LED_285 and LED_295 require approximately 30

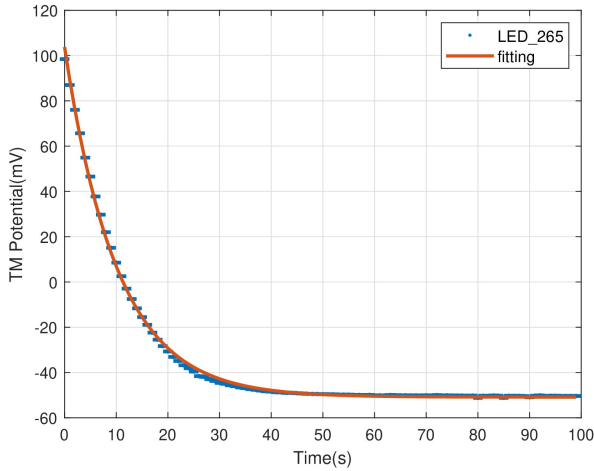


Figure 9a. LED_265.

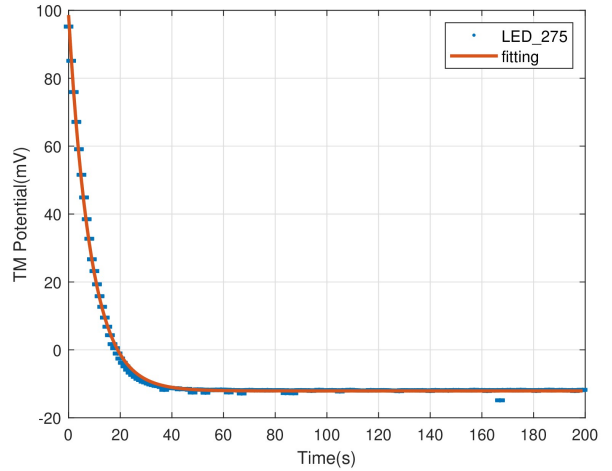


Figure 9b. LED_275.

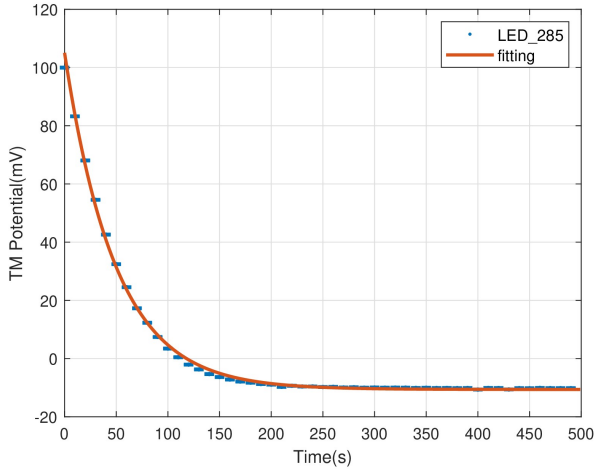


Figure 9c. LED_285.

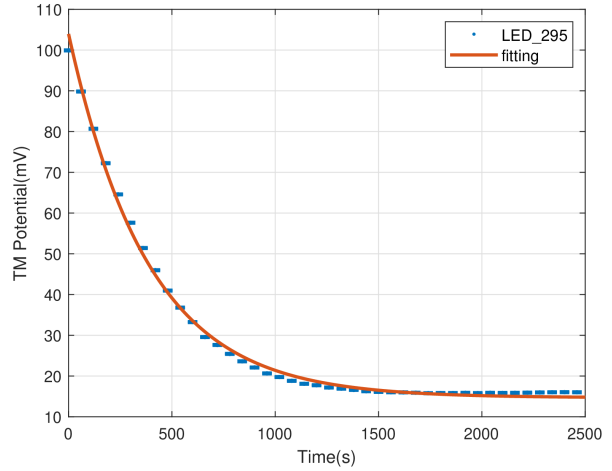


Figure 9d. LED_295.

Figure 9. TM potential variations due to photoelectrons emitted by UV-LEDs with different wavelengths. (A) LED_265. (B) LED_275. (A) LED_285. (B) LED_295.

seconds and over 600 seconds respectively, 5 times and 100 times longer than LED_265 and LED_275. This highlights a significant wavelength-dependent efficiency disparity in charge control.

While the preceding experiments utilized DC excitation currents for UV-LED operation, the methodology remains equally applicable in PWM mode. This is critical for space-based gravitational wave detectors, where DC charge control could introduce low-frequency noise into the mHz science band Weber et al. (2007). Fig. 10b(a) illustrates the potential variation of the TM through three consecutive charge-discharge cycles, employing LED_275 in PWM mode. The LED was driven at a current of 20 mA and modulated at 1 kHz with 50% duty cycle. The TM was alternately biased with a positive or negative initial potential, followed by UV-LED illumination until equilibrium was achieved in each case. This alternating sequence was repeated for three cycles, and the shaded area indicates periods of UV-LED activation.

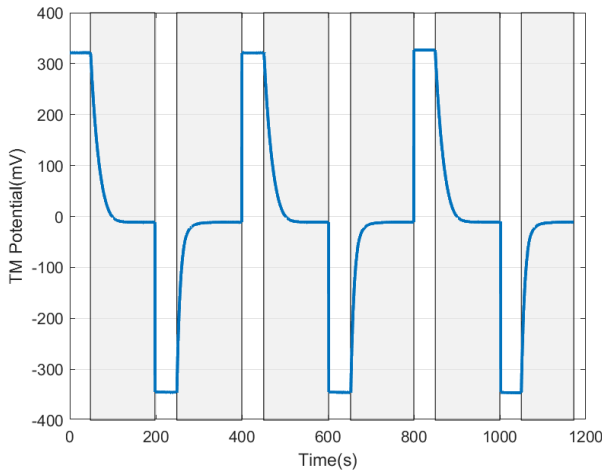


Figure 10a. Three charge control cycles.

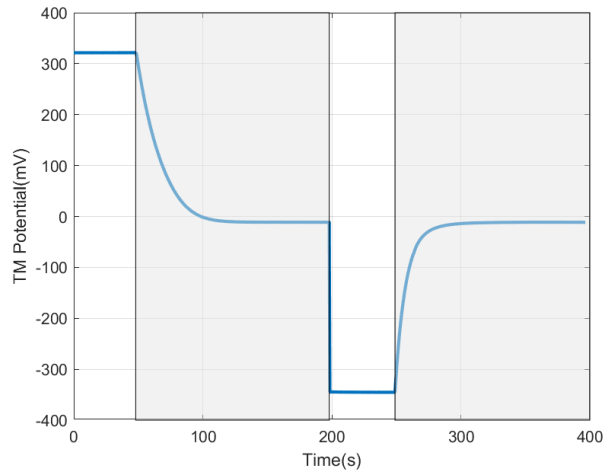


Figure 10b. Details of the first cycle.

Figure 10. Experiments utilized AC excitation currents for UV-LED operation. **(A)** Three charge control cycles. **(B)** Details of the first cycle.

The experimental results demonstrate consistent convergence of the TM potential to equilibrium under UV-LED activation across all three cycles, regardless of initial potential polarity. Fig. 10b(b) details the transient behavior of the first cycle (0 - 400 s), revealing charge and discharge phases from the initial potentials to equilibrium. This bipolar charge control demonstrates the robustness of the methodology, as demonstrated in the previous research Wang et al. (2022); Saraf et al. (2014).

The experimental results demonstrate that for gold-coated surfaces, the LED_265 showed performance comparable to the LED_255, and the LED_275, LED_285 and LED_295 exhibit a lower equilibrium potential (within 20 mV) compared to the LED_255, while wavelengths approaching 300 nm and beyond are ineffective due to insufficient photon energy. Moreover, LED_275 seems to be an optimal candidate for the source of charge management system, not only achieving a smaller equilibrium potential compared to LED_255 and LED_265 but also demonstrating a shorter time constant than long-wavelength UV-LEDs, such as LED_285 or LED_295. It should be clarified that our approach does not entirely replace the 255nm UV-LED with the 275nm variant. Instead, it offers more options for neutralizing cosmic ray charging, pending on the solar activity. On board, both the 255nm and 275nm should be placed at the four bottom corners of the caging. Depending on the intensity of the solar energetic particles and possibly contamination of the test mass, UV-LED of appropriate wavelengths will be activated for charge management.

5 CONCLUSIONS.

Based on a model of inertial sensor that mimics the surface properties and work function of a TM for LISA, UV-LEDs with multiple wavelengths were tested to evaluate their performance in continuous charge management, in terms of both the equilibrium potential and long-term stability. Additionally, the discharge rates (time constant) of UV-LEDs with different wavelengths were measured. The results show that LED_275 appears to be the best choice if optimizing for both these parameters. These results demonstrate that the 275 nm UV-LED is a promising candidate for the continuous charge management and at the same time for regular rapid discharge operation.

It is our hope that our work will provide useful input when it comes to the system design and optimisation of the charge management system in the engineering phase of a mission to detect gravitational waves in space.

CONFLICT OF INTEREST STATEMENT

The authors declare that the research was conducted in the absence of any commercial or financial relationships that could be construed as a potential conflict of interest.

AUTHOR CONTRIBUTIONS

Y.K.L., Z.L., and H.H. participated in the design and interpretation of the reported experiments or results. Y.J. and Y. Z. participated in the acquisition and/or analysis of data. Y.J., Y.Z., Z.L., and Y.K.L. participated in drafting and/or revising the manuscript. Y.J., Y.Z., Z.Z., Y.Z., H.L. and S.H. contributed to the experimental data analysis. G.C., H.H., and Z.L. provided administrative, technical, or supervisory support.

FUNDING

This work was supported by the National Key R&D Program of China (Task No. 2022YFC2204101).

DATA AVAILABILITY STATEMENT

The data used to support the findings of this study are available from the corresponding author upon reasonable request.

REFERENCES

Antonucci, F., Cavalleri, A., Dolesi, R., Hueller, M., Nicolodi, D., Tu, H. B., et al. (2012). Interaction between stray electrostatic fields and a charged free-falling test mass. *Phys. Rev. Lett.* 108. doi:10.1103/PhysRevLett.108.181101

Araújo, H., Wass, P., Shaul, D., Rochester, G., and Sumner, T. J. (2005). Detailed calculation of test-mass charging in the lisa mission. *Astroparticle Physics* 22, 451–469

Armano, M., Audley, H., Auger, G., Baird, J. T., Binetruy, P., Born, M., et al. (2017). Charge-induced force noise on free-falling test masses: Results from lisa pathfinder. *Phys. Rev. Lett.* 118, 171101. doi:10.1103/PhysRevLett.118.171101

Armano, M., Audley, H., Baird, J., Binetruy, P., Born, M., Bortoluzzi, D., et al. (2018). Precision charge control for isolated free-falling test masses: Lisa pathfinder results. *Phys. Rev. D* 98, 062001. doi:10.1103/PhysRevD.98.062001

Armano, M., Audley, H., Baird, J., Binetruy, P., Born, M., Bortoluzzi, D., et al. (2023). Charging of free-falling test masses in orbit due to cosmic rays: Results from lisa pathfinder. *Phys. Rev. D* 107, 062007. doi:10.1103/PhysRevD.107.062007

Buchman, S., Quinn, T., Keiser, G., Gill, D., and Sumner, T. (1995). Charge measurement and control for the gravity probe b gyroscopes. *Review of Scientific Instruments* 66, 120–129. doi:10.1063/1.1145276

Carbone, L., Cavalleri, A., Dolesi, R., Hoyle, C. D., Hueller, M., Vitale, S., et al. (2004). Characterization of disturbance sources for lisa: torsion pendulum results. *Classical and Quantum Gravity* 22, S509 – S519

Hollington, D., Baird, J., Sumner, T., and Wass, P. (2015). Characterising and testing deep uv leds for use in space applications. *Classical and Quantum Gravity* 32. doi:10.1088/0264-9381/32/23/235020

Hu, W.-R. and Wu, Y.-L. (2017). The taiji program in space for gravitational wave physics and the nature of gravity. *National Science Review* 4, 685–686. doi:10.1093/nsr/nwx116

Jafry, Y., Sumner, T. J., and Buchman, S. (1996). Electrostatic charging of space-borne test bodies used in precision experiments. *Classical and Quantum Gravity* 13, A97

Jia, Y., Zhang, Z., Zhang, Y., Gu, Y., Wang, S., Chai, G., et al. (2025). Test mass charge management in the detection of gravitational waves in space based on ultraviolet micro-light-emitting diode. *Space: Science & Technology* 5, 0338. doi:10.34133/space.0338

Jiang, X., Berglund, C. N., Bell, A. E., and Mackie, W. A. (1998). Os3: Photoemission from gold thin films for application in multiphotocathode arrays for electron beam lithography. *Journal of Vacuum Science & Technology B: Microelectronics and Nanometer Structures Processing, Measurement, and Phenomena* 16, 3374–3379. doi:10.1116/1.590462

Li, H., Zhou, R., Hong, W., Tian, P., Liu, L., Zhang, D., et al. (2025). Micro-led embedded uv discharge solution for space charge management. *IEEE Sensors Journal* 25, 5417–5424. doi:10.1109/JSEN.2024.3520127

Luo, J., Chen, L.-S., Duan, H.-Z., Gong, Y.-G., Hu, S., Ji, J., et al. (2016). Tianqin: a space-borne gravitational wave detector. *Classical and Quantum Gravity* 33. doi:10.1088/0264-9381/33/3/035010

Olatunde, T., Shelley, R., Chilton, A., Serra, P., Ciani, G., Mueller, G., et al. (2015). 240 nm uv leds for lisa test mass charge control. In *10TH INTERNATIONAL LISA SYMPOSIUM* (Inst High Energy Phys & Astrophys; Dept Phys; Dept Mech & Aerosp Engn; Coll Liberal Arts & Sci; Off Sponsored Res), vol. 610 of *Journal of Physics Conference Series*. doi:10.1088/1742-6596/610/1/012034. 10th International LISA Symposium, Univ Florida, Gainesville, FL, MAY 18-23, 2014

Pi, X., Liu, Q., Xu, J., Zhu, L., Wang, Q., Zhang, Y., et al. (2023). Continuous charge management scheme for tianqin. *Classical and Quantum Gravity* 40. doi:10.1088/1361-6382/acafce

Saraf, S., Balakrishnan, K., Buchman, S., Byer, R. L., Faeid, D., Hanson, J., et al. (2014). Uv led charge control of an electrically isolated proof mass in a gravitational reference sensor configuration at 255nm. In *Latin America Optics and Photonics Conference* (Optica Publishing Group), LM2A.4. doi:10.1364/LAOP.2014.LM2A.4

Saraf, S., Buchman, S., Balakrishnan, K., Lui, C. Y., Soulage, M., Faeid, D., et al. (2016). Ground testing and flight demonstration of charge management of insulated test masses using uv-led electron photoemission. *Classical and Quantum Gravity* 33, 245004. doi:10.1088/0264-9381/33/24/245004

Schulte, M. O., Shaul, D. N. A., Hollington, D., Waschke, S., Sumner, T. J., Wass, P. J., et al. (2009). Inertial sensor surface properties for lisa pathfinder and their effect on test mass discharging. *Classical and Quantum Gravity* 26, 094008. doi:10.1088/0264-9381/26/9/094008

Sumner, T. J., Mueller, G., Conklin, J. W., Wass, P. J., and Hollington, D. (2020). Charge induced acceleration noise in the lisa gravitational reference sensor. *Classical and Quantum Gravity* 37, 045010. doi:10.1088/1361-6382/ab5f6e

Sumner, T. J., Shaul, D. N. A., Schulte, M. O., Waschke, S., Hollington, D., and Araujo, H. (2009). Lisa and lisa pathfinder charging. *Classical and Quantum Gravity* 26. doi:10.1088/0264-9381/26/9/094006. 7th International LISA Symposium, Barcelona, SPAIN, JUN 16-20, 2008

Wang, S., Saraf, S., Lipa, J., Yadav, D., and Buchman, S. (2022). Two approaches for the passive charge management of contactless test masses. *Classical and Quantum Gravity* 39, 195008. doi:10.1088/1361-6382/ac838e

Wass, P. J., Carbone, L., Cavalleri, A., Ciani, G., Dolesi, R., Hueller, M., et al. (2006). Testing of the uv discharge system for lisa pathfinder. In *LASER INTERFEROMETER SPACE ANTENNA*, eds. S. Merkowitz and J. Livas (NASA Goddard Space Flight Ctr), vol. 873 of *AIP Conference Proceedings*, 220+. 6th International Laser Interferometer Space Antenna, Greenbelt, MD, JUN 19-23, 2006

Weber, W. J., Carbone, L., Cavalleri, A., Dolesi, R., Hoyle, C. D., Hueller, M., et al. (2007). Possibilities for measurement and compensation of stray dc electric fields acting on drag-free test masses. *ADVANCES IN SPACE RESEARCH* 39, 213–218. doi:10.1016/j.asr.2006.03.045

Yang, F., Bai, Y., Hong, W., Sumner, T. J., and Zhou, Z. (2020). A charge control method for space-mission inertial sensor using differential uv led emission. *Review of Scientific Instruments* 91, 124502. doi:10.1063/5.0013232